Fibers and Polymers 2014, Vol.15, No.11, 2253-2259 DOI 10.1007/s12221-014-2253-x

Electrical Characteristics of Au/PVA (x-doped)/n-Si: Comparison Study on the Effect of Dopant Type in PVA

İlbilge Dökme* and Şemsettin Altındal

Science Education Department, Faculty of Gazi Education, Gazi University, Ankara, Turkey
(Received May 3, 2011; Revised August 19, 2011; Accepted September 4, 2011)

Abstract: The main propose of this study is to investigate whether the doppant material in PVA would change the electrical characteristics of Au/PVA (X-doped) n-Si Schottky structure. Therefore, Au/PVA (Co, Zn-doped) n-Si (D1) and /PVA (Co, Ni-doped) n-Si (D2) Schottky structures were fabricated under the same condition using n-type (phosphor-doped) single crystal silicon wafer with (111) surface orientation. After the PVA/(Co-Zn) and PVA/(Co-Ni) acetates was obtained, the nanofiber film was fabricated on the silicon wafer by the use of an electrospinning technique. The results indicated that the electrical parameters of Au/PVA (x-doped) n-Si Schottky structure were significantly influenced from the doppant material in PVA. Comparative results on electrical parameters of D1 and D2 were reported in this study.

Keywords: Au/PVA(x-doped)/n-Si, Nanofiber, Schottky diode, Polyvinyl alcohol, Electrospinning technique

Introduction

Metal/organic polymer/semiconductor structures became attractive for applications in electronic and optoelectronic devices such as all polymer integrated circuits [1], sensors [2], field effect transistors (FETs), Schottky diodes (SDs), light emitting diodes (LEDs), etc. [3]. There have been a large number of studies on SDs with polymeric interfacial layer in the literature [4-20]. Actually, this has opened a new opportunity of replacing conventional inorganic devices by the organic ones. For an interfacial layer of SDs, various polymers such as polyaniline, poly(alkylthiophene), polypyrrole, polythiophene, poly(3-hexylthiophene), and polyvinyl alcohol (PVA) are of great attractive research topic because of their potential applications and interesting properties by chemists, physicists, and electrical engineers as well. Among them, in recent years, PVA nanofabrics have attracted much attention due to its unique chemical and physical properties as well as its industrial applications [21-29].

PVA has normally a poor electrical conductivity and becomes conductive upon doping with some dopants [25,30-33]. Conductivity in PVA arises due to the high physical interactions between polymer chains, via hydrogen bonding between the hydroxyl groups and the dopant, and is mainly dominated by the properties of the amorphous regions. In addition, the ionic mobility in the amorphous region changes by segmental motion of the PVA host and it changes with crystallization and structural order. Hence the ionic conductivity of a doped polymer is mainly localized into the amorphous phase. The dopant may reside within the amorphous regions forming a charge transfer complex, or it may exist in the form of molecular aggregates between the polymer chains of PVA [30].

The electrical characteristics of only Au/PVA (Co, Zn-doped) n-Si (D1) were analyzed and reported in our previous study [34]. In this study, the measured electrical characteristics of Au/PVA (Co, Zn-doped) n-Si (D1) and /PVA (Co, Ni-doped) n-Si (D2) Schottky diodes were attempted to analyzed comparatively. The main propose of this study is to investigate whether the dopant material in PVA would change the electrical characteristics of Au/PVA (x-doped) n-Si Schottky structure. Therefore, each diode was fabricated under the same condition. The experimental procedure of fabrication and measurements in all detail are given following section.

*Corresponding author: ilbilgedokme@gazi.edu.tr

Experimental

The Au/PVA (Co, Zn-doped) n-Si (D1) and /PVA (Co, Ni-doped) n-Si (D2) Schottky structure were fabricated in the same condition. Schematic cross-section of the device is given in Figure 1. The detail of experimental procedure is explained step by step in following section.

Forming Ohmic Back Contact

The semiconductor used in this study was n-type (phosphor doped) single crystal silicon (111) with a thickness of 350 μm, and a resistivity of 0.7 Ω-cm. For the initial fabrication process, Si wafer was degreased in organic solution of peroxide- ammoniac solution in 10 min and then etched in a sequence of H_2O+ HCl solution and finally quenched in de-ionised water for a prolonged time. Preceding each cleaning

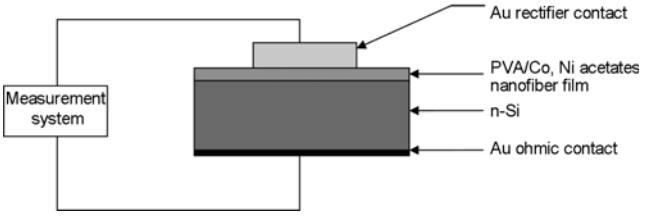


Figure 1. Schematic cross-section of the Au/PVA (x-doped) n-Si Schottky structure.

step, the wafer was rinsed thoroughly in de-ionized water of resistivity of 18 MΩ cm. Immediately, after surface cleaning, high purity (99.999 %) gold with a thickness of ~2000 Å was thermally evaporated onto the whole back side of Si wafer in the a pressure about 10^{-6} torr in high vacuum system. In order to perform a low resistivity ohmic back contact, Si wafer was sintered at 450 °C for 5 min in N_2 atmosphere. The wafer cut into two pieces and are named D1 and D2.

Preparation and Spinning of PVA

For D1, 0.5 g of cobalt acetate and 00.25 g of zinc acetate was mixed with 1 g of polyvinyl alcohol (PVA), molecular weight=72,000 and 9 m*l* of de-ionised water. After vigorous stirring for 2 h at 50 °C, a viscous solution of PVA/(Co, Zn dopped) acetates was obtained.

For D2, 0.5 g of cobalt acetate and 0.25 g of nickel acetate was mixed with 1 g of PVA, molecular weight=72,000 and 9 m*l* of de-ionised water. After vigorous stirring for 2 h at 50 °C, a viscous solution of PVA/(Co, Ni dopped) acetates was obtained.

The solution of the PVA (Co, Zn-doped) and PVA (Co, Ni-doped) was homogenized for 1.5 h by mixing with rotation before the deposition. The PVA (Co, Zn-doped) and PVA (Co, Ni-doped) nanofiber film on n-Si substare was coated by electrospinning technique. Electrospinning process utilizes electrical force to produce polymer fibers. Electrospinning setup consists of four major components: The high-voltage power supply, the spinneret, the syringe pump and the electrically conductive collector. A simple illustration of the electrospinning system is given in Figure 2. In this system, using a peristaltic syringe pump, the precursor solution was delivered to a metal needle syringe (10 m*l*) with an inner diameter of 0.9 mm at a constant flow rate of 0.02 m*l*/h. The needle was connected to a high voltage power supply and positioned vertically on a clamp. A piece of flat aluminum foil was placed 15 cm below the tip of the needle to collect the nanofibers. Si wafer was placed on the aluminum foil. Upon applying a high voltage of 20 kV on the needle, a fluid jet was ejected from the tip. The solvent evaporated and a charged fiber was deposited onto the Si wafer as a nonwoven mat.

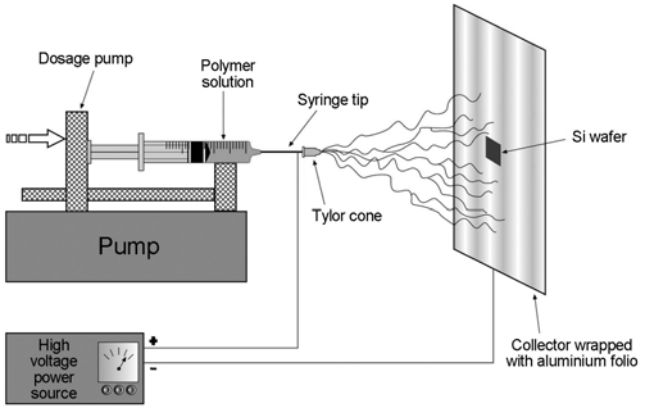


Figure 2. Schematic representation of the electrospinning process.

Fiber formation and morphology of the electrospun PVA/Co, Ni acetate fibers determined using a scanning electron microscope (SEM) Quanto 400 FEI MK-2 are given in Figure 3.

Fabricating of Schottky/rectifier Contacts and Current-voltage Measurements

After spinning process, circular dots of 1 mm in diameter and 1500 Å thick high purity Au rectifying contacts were deposited on the PVA surface of the wafer through a metal shadow mask in liquid nitrogen traped oil-free ultra high vacuum system in the pressure of about 10^{-7} torr. The forward and reverse bias *I-V* measurements were performed by the use of a Keithley 2400 source meter at the temperature of 300 and 360 K using a temperature-controlled Janis vpf-475 cryostat, which enabled us to make measurements in the temperature range of 77-450 K.

The sample temperature was always monitored by using a copper-constantan thermocouple close to the sample, and measured with a dmm/scanner Keithley model 199 and a Lake Shore model 321 auto-tuning temperature controllers

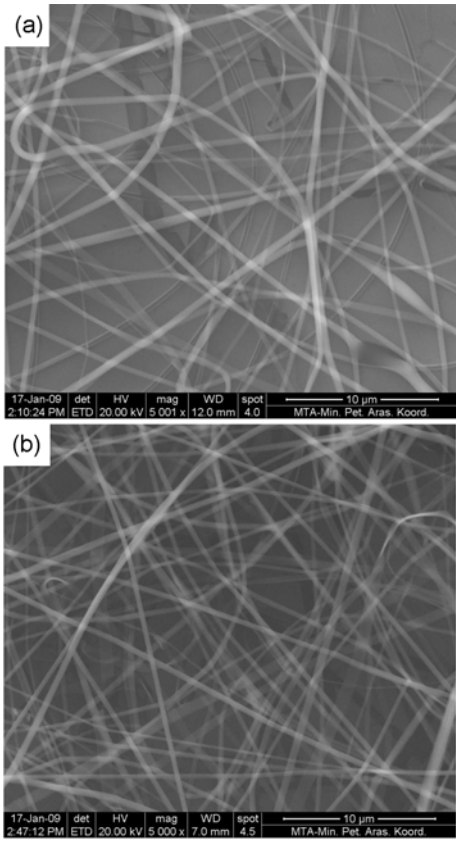


Figure 3. Selected SEM images of (a) PVA (Co, Ni, acetate) and (b) PVA/(Co, Zn acetate) nanofibers.

with sensitivity better than ±0.1 K. All measurements were carried out with the help of a microcomputer through an IEEE-488 AC/DC converter card.

Results and Discussion

For a Schottky structure with the series resistance and the ideality factor greeter than unity, the current-voltage relation based on thermionic emission (TE) theory can be expressed as [35-39]

$$I = I_o\left[\exp\frac{q}{nkT}(V - IR_s)\right] \quad (1a)$$

where V is the definite forward bias voltage, IR_s term is the voltage drop across series resistance of the device, n is the ideality factor, k is the Boltzmann constant and T is temperature in Kelvin and I_o is the reverse saturation current. The value of I_o can be obtained from the y-axis intercept of the linear region of the semi-log-forward bias I-V plots and expressed as

$$I_o = A^* A T^2 \exp(-q\Phi_{Bo}/kT) \quad (1b)$$

where the quantities A^*, A, Φ_{Bo} are the effective Richardson constant and equals to 120 A/cm^{2}K^2 for n-type Si, the diode area and, the zero-bias barrier height respectively.

Ideality factor is a measure of conformity of the diode to pure thermionic emission and is contained in the slope of straight line region of the forward bias logarithmic characteristics of I-V plot through the relation [37]

$$n = \frac{q}{kT}\left[\frac{d(V)}{dLn(I)}\right] \quad (2)$$

Figure 4(a) and (b) show the experimental semi-logarithmic I-V characteristics of the sample D1 and D2 respectively. The Φ_{Bo} and n values of SDs were calculated with the help of equations (1b) and (2) from the y-axis intercept and slope of the linear region of the semi-log-forward bias I-V plots, respectively, and they given in Table 1. The values of n for the sample D1 and D2 were found as 3.71 and 2.23 (at 300 K), and 1.66 and 2.08 (at 360 K), respectively.

The values of barrier height (BH) for the sample D1 and D2 were found as 0.74 and 0.80 eV (at 300 K), and 0.82, 0.87 eV (at 360 K), respectively.

In general, the forward bias I-V characteristic is linear on a semilogarithmic scale at low forward bias voltages but

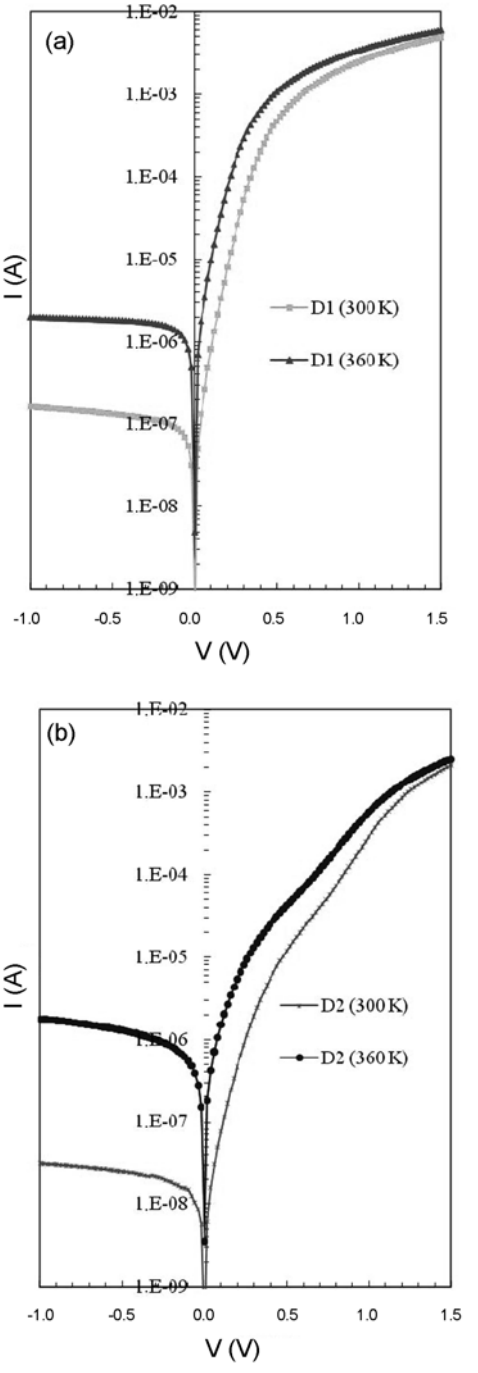


Figure 4. The experimental I-V characteristics of (a) Au/PVA (Co, Zn-doped) n-Si (D1) and (b) Au /PVA (Co, Ni-doped) n-Si (D2).

Table 1. The experimental values of diode parameters obtained from the forward I-V characteristics of D1 and D2

T (K)	Sample	n (I-V)	n ($dV/dLnI$)	Φ_{Bo} (I-V) (eV)	Φ_{Bo} (H(I)) (eV)	R_s (dV/dLnI) (Ω)	R_s(H(I)) (Ω)
300 K	D1	1.92	1.81	0.74	0.60	230.52	254.82
	D2	2.23	2.08	0.80	0.83	166.59	166.80
360 K	D1	1.66	1.38	0.82	0.83	189.38	184.00
	D2	2.08	1.86	0.87	0.96	192.01	189.69

deviates considerably from linearity due to the effect of series resistance (R_s), the interfacial layer, and the interface states when the applied voltage is sufficiently large. The series resistance is important in the downward curvature of the forward bias *I-V* characteristics, while the other two parameters are important in both linear and non-linear regions of *I-V* characteristics. Therefore the values of n, Φ_{Bo}, R_s are evaluated using a method developed by Cheung and Cheung [40] in the high current range where the *I-V* characteristic is not linear. According to this method from equation (1a), the following functions can be written as

$$\frac{dV}{dLnI} = n\frac{kT}{q} + IR_s \tag{3}$$

$$H(I) = V + n\frac{kT}{q}Ln\left(\frac{I}{AA^*T^2}\right) \tag{4}$$

and $H(I)$ is given as follows $H(I) = n\Phi_{Bo} + IR_s$ (5)

Experimental $dV/d(LnI)$ vs I and $H(I)$ vs I plots for D1 and D2 at 300 and 360 K are presented in Figures 5 and 6 respectively. Equation (3) should give a straight line for the data of downward curvature region in the forward bias *I-V* characteristic. Thus, a plot of $dV/d(LnI)$ vs I will give R_s as the slope and nkT/q as the y-axis intercept. Using the n value determined from equation (3) and the data of downward curvature region in equation (4), a plot of $H(I)$ vs. I according to equation (5) will also give a straight line with y-axis intercept equal to $n\Phi_{Bo}$. From $dV/d(\ln I)$ vs. I plot by means of equation (3), the values of R_s and n of sample D1 and D2 are given in Table 1. The values of Φ_{Bo} and R_s from $H(I)$-I plot according to equation (5) are also seen in this table.

The Φ_{Bo} values of the samples D1 and D2 were calculated as 0.60 and 0.83 eV at 300 K respectively. A similar increase was also observed at 360 K. The barrier height values of D1 are lower than those of D2 although the polymeric interfacial layer thickness of D1 and D2 are same. It can be explained only additional effect caused by dopant type in polymeric interfacial layer.

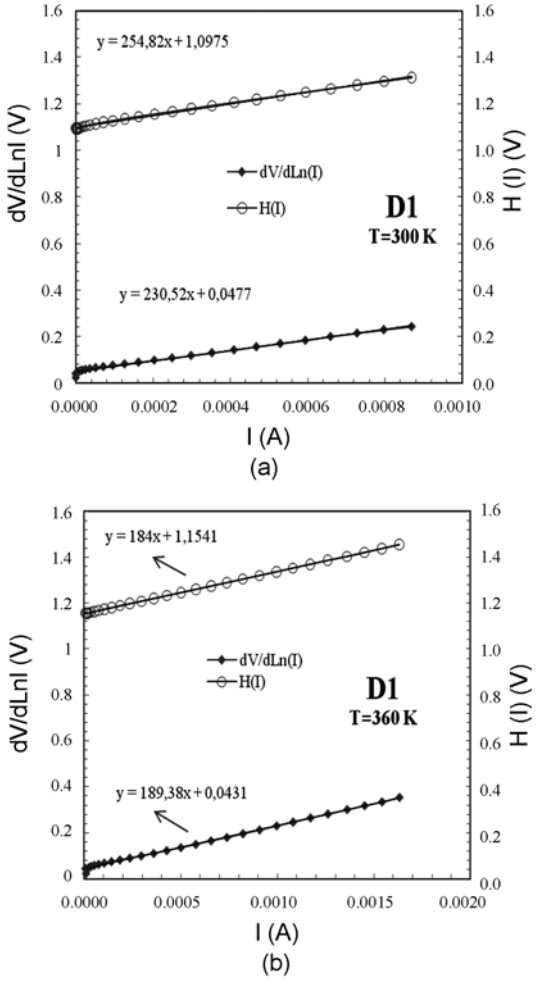


Figure 5. The dV/dln (I) vs. I and $H(I)$ vs. I plots for D1 at (a) 300 K and (b) 360 K.

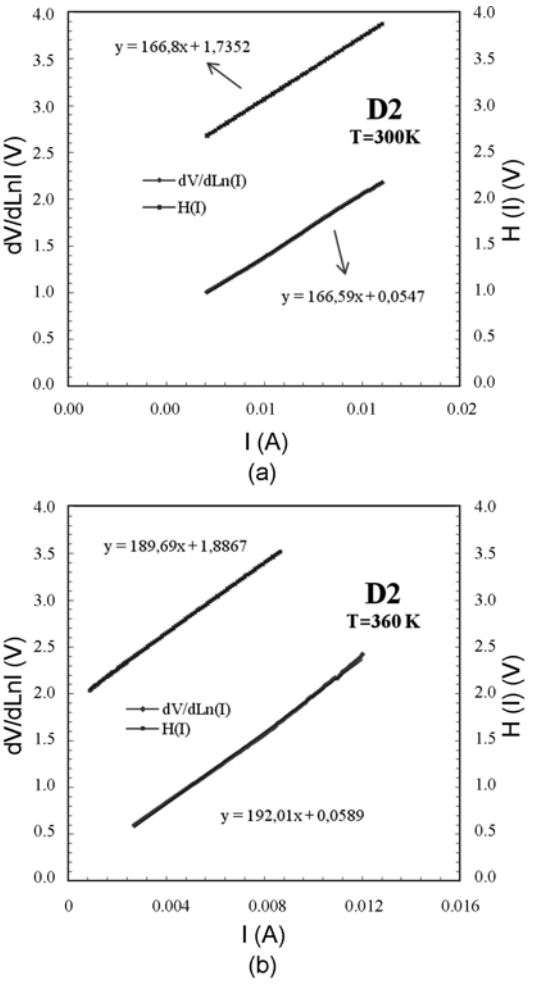


Figure 6. The dV/dln (I) vs. I and $H(I)$ vs. I plots for D2 at (a) 300 K and (b) 360 K.

The R_s values of D1 and D2 calculated by different techniques are in good agreement with each other (Table 1). The R_s values of D1 have been found to be higher than that of D2 at each temperature. Furthermore, the R_s values of D1 at 360 K are lower than that of D1 at 300 K. However, the R_s values of D2 at 360 K are higher than that of D2 at 300 K. This can be attributed to the type of dopant material in PVA of devices. D1 with Co, Zn material in PVA as an dopant material behave as an semiconductor while D2 with Co, Ni material in PVA behave as an conductor.

As seen in Table 1, the values of n calculated from thermionic emission theory are poorer than those calculated from Cheung function [40]. At two temperatures the n values of the sample D1 has been found to be smaller than those of the sample D2. The amount of n greater than unity can arise from the variation of barrier height (Φ_{Bo}) with applied voltage, which lead to extra current mechanism such as thermionic-field emission, generation-recombination, tunneling [35,41]. However the lightly doped semiconductors generally requiring Schottky diodes offer R_s and so a significant voltage drop occurs across that at large forward bias region. The interface states density (N_{ss}) is also important effect for high value of ideality factor [42,43]. The sufficiently thick interface layer disconnects the interface states from the metal, making them communicate with the semiconductor more readily than with the metal. D1 and D2 are the same thickness of polymeric interfacial layer. In spite of the same thickness of polymeric interfacial layer and the same type of polymer (PVA) the diversity in the parameters of D1 and D2 show clear evidence for interface states and series resistance effects changing by the fact the dopant type in PVA. Less information exists about interface states in organic materials for Schottky structure. Stallinga *et al.* [44] and Berleb *et al.* [45] use admittance spectroscopy to find evidence for trapped charge at an organic-organic interface, but no information is found as to the distribution of these charges in energy. Here, we obtained the energy density distribution profile of interface states from the forward *I-V* characteristics of D1 and D2 [41]. Since the values of ideality factor and barrier height are assumed to be voltage dependent, for a Schottky structure with interface states governed by the semiconductor, the expression for the density of interface states as deduced by Card and Rhoderick [41] can be written following equations

$$n(V) = \frac{q}{kT}\left[\frac{V}{Ln(I/I_o)}\right] \tag{6a}$$

$$\Phi_e = \Phi_{Bo} + \beta(V) = \Phi_{Bo} + \left(1 - \frac{1}{n(V)}\right)V \tag{6b}$$

$$N_{ss}(V) = \frac{1}{q}\left[\frac{\varepsilon_i}{\delta}(n(V)-1) - \frac{\varepsilon_s}{W_D}\right] \tag{6c}$$

where β is the voltage coefficient of the effective barrier height Φ_e, δ is the thickness of interfacial layer calculated equation (10) in ref [34], W_D is the width of the space charge region (obtained from the experimental C^{-2} vs V plots at 100 kHz), e_i and e_s are permittivity of the interfacial insulator layer and the semiconductor, respectively, and N_{ss} is the density of the interface states in equilibrium with the semiconductor, respectively.

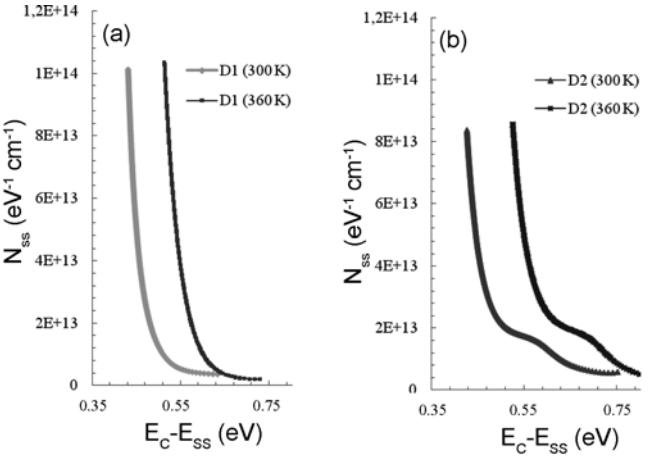


Figure 7. The interface states energy distribution curves of (a) D1 and (b) D2 at 300 and 360 K.

The energy of the interface states E_{ss} (for n-type semiconductors) with respect to the bottom of the conduction band at the surface of semiconductor is given by [4,35]

$$E_c - E_{ss} = q(\Phi_e - V) \tag{7}$$

Figure 7(a) shows the energy distribution profile of the N_{ss} obtained from the forward bias *I-V* characteristics of D1 by taking into account effective BH (Φ_e) at 300 and 360 K respectively. As can be seen this figure, the exponential growth of the N_{ss} from midgap towards the bottom of conduction band is very apparent [43]. The energy values of the density distribution the N_{ss} are in the range (E_c−0.43) to (E_c−0.64) eV for D1 at 300 K. The values of the N_{ss} in (E_c−0.43) and (E_c−0.64) are 1.03×10^{14} and 3.6×10^{12} eV^{-1} cm^{-2}, respectively. The energy values of the density distribution the N_{ss} are in the range (E_c−0.51) to (E_c−0.73) eV for D1 at 360 K. The values of the N_{ss} in (E_c−0.51) and (E_c−0.73) are 1.03×10^{14} and 1.91×10^{12} eV^{-1} cm^{-2}, respectively.

The energy distribution profile of the N_{ss} obtained from the forward bias *I-V* characteristics of D2 at 300 and 360 K is given in Figure 7(b), respectively. The energy values of the density distribution the interface states are in the range (E_c−0.42) to (E_c−0.75) eV for D2 at 300 K. The values of the N_{ss} in (E_c−0.42) and (E_c−0.75) are 8.19×10^{13} and 5.88×10^{12} eV^{-1} cm^{-2}, respectively. The energy values of the density distribution the N_{ss} are in the range (E_c−0.52) to (E_c−0.81) eV for D2 at 360 K. The values of the N_{ss} in (E_c−0.52) and (E_c−0.81) are 8.48×10^{13} and 4.53×10^{12} eV^{-1} cm^{-2}, respectively.

Conclusion

The semilogarithmic forward and reverse bias *I-V* characteristics of Au/PVA (Co, Zn-doped) n-Si (D1) and /PVA (Co, Ni-doped) n-Si (D2) Schottky structures fabricated under same condition were measured at 300 and 360 K in this study. Electrical parameters of these two diodes were calculated and compared with each other for these two temperatures. It was found that n and Φ_B values of D1 were lower than those of D2 at the two temperatures. The R_s value of the D1 was higher than that of D2 at 300 K while the R_s value of the D2 was smaller than that of D2 at 360 K. The energy distribution profile of the N_{ss} obtained from the forward bias *I-V* characteristics by taking into account the effective BH (Φ_e) of D1 and D2 are not to be found same. The N_{ss} of D1 and D2 at 300 K changed from 1.03×10^{14} to 3.6×10^{12} eV^{-1} cm^{-2} and 8.19×10^{13} to 5.88×10^{12} eV^{-1} cm^{-2} respectively. However, at 360 K the N_{ss} of D1 and D2 changed from 1.03×10^{14} to 1.91×10^{12} eV^{-1} cm^{-2} and 8.48×10^{13} to 4.53×10^{12} eV^{-1} cm^{-2}, respectively. All results indicated that the electrical parameters of Au/PVA (x-doped) n-Si Schottky structure were significantly influenced dopant material in PVA. However, the detail of the effect of dopant type and the ratio of doped material in PVA on electrical characteristics of Schottky devices is unclear. Further research is required to solve this problem. Therefore Schotkky devices with polymeric interfacial layer should be produced a more systematic way. The next research we planned will include in fabricating Schottky devices by controlling same fabrication variables and changing a single variable systematically. Hence, during the fabricating process, a) while the type of polymer, the ratio of doped material and the thickness of polymer film will be constant, the type of single doped material will be changed systematically, b) the type of polymer, the type of doped material and the thickness of polymer film will be constant, the ratio of doped material will be changed systematically.

Acknowledgements

This work is supported by Gazi University Scientific Research Project numbered 04/2010-27.

References

1. A. R. Brown, C. P. Jarret, D. M. de Leeuw, and M. Matters, *Synth. Met*., **88**, 37 (1997).
2. B. K. Crone, A. Dodabalapur, R. Sarpeshkar, A. Gelperin, H. E. Katz, and Z. Bao, *J. Appl. Phys.,* **91**, 10140 (2002).
3. F. Gutman and L. E. Lyons, "Organic Semiconductors", Wiley, New York, 1967.
4. Ö. Güllü, Ş. Aydoğan, and A. Türüt, *Microelecron. Engineering*, **85**, 1647 (2008).
5. B. Abay, Y. Onganer, M. Sağlam, H. Efeoğlu, A. Türüt, and Y. K. Yoğurtçu, *Microelecron. Engineering*, **51-52**, 689 (2000).
6. M. Çakar, C. Temirci, and A. Türüt, *Synth. Met.*, **142**, 177 (2004).
7. Y. Onganer, M. Sağlam, A. Türüt, H. Efeoğlu, and S. Tüzemen, *Solid-State Electron*., **39**, 677 (1996).
8. K. Akkılıç, M. E. Aydın, İ. Uzun, and T. Kılıçoğlu, *Synth. Met.*, **156**, 958 (2006).
9. K. S. Kang, Y. Chen, H. K. Lim, K. Y. Cho, K. J. Han, and J. Kim, *Thin Solid Films*, **517**, 6096 (2009).
10. A. Takshi, M. Mohammadi, and J. D. Madden, *Solid-State Electron*., **52**, 1717 (2008).
11. Ö. Güllü, Ö. Barış, M. Biber, and A. Türüt, *Appl. Surf. Sci*., **254**, 3039 (2008).
12. A. Assadi, C. Svensson, M. Willander, and O. Inganäs, *J. Appl. Phys*., **72**, 2900 (1992).
13. T. Kılıçoğlu, M. E. Aydın, and Y. S. Ocak, *Physica B: Con. Matt*., **388**, 242 (2007).
14. M. E. Aydın, T. Kılıçoğlu, A. Akkılıç, and H. Hoşgören, *Physica B: Con. Matt*., **381**, 113 (2006).
15. İ. Dökme, Ş. Altındal, T. Tunç, and İ. Uslu, *Microelectron. Reliab*., **50**, 39 (2010).
16. F. Yakuphanoğlu, *Synth. Met.*, **160**, 1551 (2010).
17. F. Yakuphanoğlu, *Synth. Met.*, **158**, 108 (2008).
18. F. Yakuphanoğlu and B. F. Şenkal, *Synth. Met.*, **159**, 311 (2009).
19. M. E. Aydin, F. Yakuphanoğlu, and G. Öztürk, *Synth. Met.*, **160**, 2186 (2010).
20. F. Yakuphanoğlu and R. S. Anand, *Synth. Met.*, **160**, 2250 (2010).
21. J. Zhang and F. Jiang, *Chem. Phys.*, **289**, 243 (2003).
22. N. Dharmaraj, C. H. Kim, and H. Y. Kim, *Synth. React. Inorg. Met.-Org. Chem*., **36**, 29 (2006).
23. G. V. Bazuev, O. I. Gyrdasova, I. G. Grigorov, and O. V. Koryakova, *Inorg. Mater.,* **41**, 288 (2005).
24. H. Guan, C. Shao, S. Wen, B. Chen, J. Gong, and X. Yang, *Mater. Chem. Phys*., **82**, 1002 (2003).
25. I. Uslu, B. Başer, A. Yaylı, and M. L. Aksu, *e-Polymers*, **7**, 1699 (2007).
26. I. Uslu, H. Daştan, A. Altas, A. Yayli, O. Atakol, and M. L. Aksu, *e-Polymers,* **7**, 1568 (2007).
27. H. Saito and B. Stuhn, *Polymer*, **35**, 475 (1994).
28. M. M. Mosaad, *J. Mater. Sci. Lett.,* **9**, 32 (1990).
29. A. H. Salama, M. Dawy, and A. M. A. Nada, *Polymer-Plast. Technol. Eng*., **43**, 1067 (2004).
30. R. F. Bhajantri, V. Ravindrachary, A. Harisha, C. Ranganathaiah, and G. N. Kumaraswamy, *Appl. Phys. A-Mater.,* **87**, 797 (2007).
31. A. Shehap, A. Abdallah, A. F. Basha, and F. H. Abd el Kader, *J. Appl. Polym. Sci.,* **68**, 687 (1998).
32. H. M. Zidan, *J. Appl. Polym. Sci.,* **88**, 104 (2003).
33. D.-H. Wang, *Thin Solid Films*, **288**, 254 (1996).
34. İ. Dökme, Ş. Altındal, T. Tunç, and İ. Uslu, *Synthetic Metals*, **161**, 474 (2011).

35. E. H. Rhoderick and R. H. Williams, "Metal-Semiconductor Contacts", 2nd ed., Clarendon Press, Oxford, 1988.
36. S. M. Sze, "Physics of Semiconductor Devices", 2nd ed., p.850, Willey, New York, 1981.
37. H. Norde, *J. Appl. Phys*., **50**, 5052 (1979).
38. N. Yıldırım, K. Ejderha, and A. Türüt, *J. Appl. Phys*., **108**, 11450 (2010)
39. A. Singh, *Solid State Electron*., **28**, 223 (1985).
40. S. K. Cheung and N. W. Cheung, *Appl. Phys. Lett*., **49**, 85 (1986).
41. H. C. Card and E. H. Rhoderick, *J. Phys. D: Appl. Phys*., **4**, 1589 (1971).
42. M. E. Aydin, F. Yakuphanoglu, J. Eom, and D. Hwang, *Physica B*, **387**, 239 (2007).
43. F. Yakuphanoğlu, *J. Phys. Chem. C*, **111**, 1505 (2007).
44. P. Stallinga, H. L. Gomes, M. Murgia, and K. Müllen, *Organic Electronics,* **3**, 43 (2002).
45. S. Berleb, W. Brütting, and G. Paasch, *Organic Electronics*, **1**, 41 (2000).